TU Delft

Delft University of Technology

Drivers of cross-shore chenier dynamics off a drowning coastal plain

Tas, Silke A.J.; van Maren, Dirk S.; Helmi, Muhammad; Reniers, Ad J.H.M.

DOI
10.1016/j.margeo.2022.106753

Publication date
2022

Document Version
Final published version

Published in
Marine Geology

Citation (APA)
Tas, S. A. J., van Maren, D. S., Helmi, M., & Reniers, A. J. H. M. (2022). Drivers of cross-shore chenier dynamics off a drowning coastal plain. *Marine Geology*, *445*, Article 106753. https://doi.org/10.1016/j.margeo.2022.106753

Important note
To cite this publication, please use the final published version (if applicable).
Please check the document version above.

Copyright
Other than for strictly personal use, it is not permitted to download, forward or distribute the text or part of it, without the consent of the author(s) and/or copyright holder(s), unless the work is under an open content license such as Creative Commons.

Takedown policy
Please contact us and provide details if you believe this document breaches copyrights.
We will remove access to the work immediately and investigate your claim.

This work is downloaded from Delft University of Technology.
For technical reasons the number of authors shown on this cover page is limited to a maximum of 10.

Marine Geology 445 (2022) 106753

Contents lists available at ScienceDirect

Marine Geology

journal homepage: www.elsevier.com/locate/margo

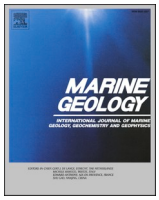

Research Article

Drivers of cross-shore chenier dynamics off a drowning coastal plain

Silke A.J. Tas [a,*], Dirk S. van Maren [a,b,c], Muhammad Helmi [d], Ad J.H.M. Reniers [a]

[a] Faculty of Civil Engineering and Geosciences, Delft University of Technology, Stevinweg 1, Delft 2628 CN, the Netherlands
[b] State Key Lab of Estuarine and Coastal Research, East China Normal University, 500 Dongchuan Rd, Shanghai 200062, China
[c] Deltares, P.O. Box 177, Delft 2600 MH, the Netherlands
[d] Faculty of Fisheries and Marine Science, Universitas Diponegoro, Jl. Prof. H. Soedarto, Semarang 50275, Indonesia

ARTICLE INFO

Editor: Prof. Edward Anthony

Keywords:
Cheniers
Modelling
Morphodynamics
Tide
Waves

ABSTRACT

A chenier is a beach ridge, consisting of sand and/or shells, overlying a muddy substrate. In this paper, we explore the cross-shore dynamics of cheniers in their 'active' phase, i.e. the phase between their formation and their landing on the shore and can no longer be reached by daily wave and tidal influences. While cheniers described in literature are known to only migrate onshore until they reach a stable position with their crest level above tidal influences, observations in Demak suggest the existence of an alternative stable state, highly dynamic on the short term, but stable on the longer term. To explore this alternative stable state, we developed an idealised chenier model to investigate cross-shore chenier dynamics under daily wave and tidal influences. The model is able to predict both onshore and offshore migration; onshore migration is mainly driven by wave action, while offshore migration is induced by a tidal phase lag, or the effect of the storm season. For certain combinations of waves, tide (incl. phase lag) and a storm season effect, the model predicts a dynamically stable chenier. In absence of a phase lag and storm season effect, the model yields a 'classic' stable chenier that welds onto the shoreline by onshore migration.

1. Introduction

Cheniers are traditionally defined as ridges consisting of wave-reworked coarse-grained sediments, resting on top of muddy sediment, separated from the shoreline by a mudflat (Augustinus, 1989; Otvos and Price, 1979). While Otvos (2019) argues that the term 'chenier' may only be applied to ridges that are 'stranded', i.e. they are fixated between mudflats on both the landward and seaward side, and therefore are no longer influenced by daily wave and tidal processes, the term is also widely used for 'active cheniers', whose crest is still low enough to experience (occasional) overwash and can be considered dynamic. Some examples of active cheniers are the cheniers in the interbank phase along the coast of the Guianas (Anthony et al., 2010, 2013, 2019; Nardin and Fagherazzi, 2018; Augustinus, 1980; Brunier et al., 2019; Toorman et al., 2018), the cheniers that developed after the construction of a dike in Gomso Bay, Korea (Lee et al., 1994; Ryu et al., 2008), cheniers in the Firth of Thames, New Zealand (Woodroffe et al., 1983), and the cheniers forming the Saltés Island Chenier Plain in Spain (Morales et al., 2014). In this paper we use this more generous interpretation of the term 'chenier' to include the active sandy ridges in a muddy intertidal zone.

Cheniers are usually found on mildly sloping coasts with a low to moderate wave-energy environment (Augustinus, 1989). Their formation depends on a specific balance between wave action and sediment availability and is generally episodic (Otvos and Price, 1979; Nardin and Fagherazzi, 2018; Anthony et al., 2019). Contrary to beach ridges found on sandy shores, which are built up from material similar in composition to the adjacent beach and shoreface (Taylor and Stone, 1996), the volume of a chenier is limited by the availability of coarser particles in the otherwise muddy shoreface (Anthony et al., 2019). As a result, when ridges are subjected to wave action, beach ridges may be able to build out both horizontally and vertically, but cheniers usually start migrating landward (and alongshore) instead of building up, due to the lack of additional sediment. Generally, cheniers continue to migrate landward by washover processes at a decelerating rate, until their crest is above spring tide or storm surge level (Augustinus, 1980, 1989; Morales et al., 2014; Rhodes, 1982; Woodroffe et al., 1983; Woodroffe and Grime, 1999). Only in the rare occasions when sufficient coarse sediment is available, cheniers are able to grow in volume and elevation, reducing sediment transport resulting from overwash processes and the resulting landward migration rate (Neal et al., 2002). For situations with sufficient sediment availability, the cheniers may then prograde seaward

* Corresponding author.
E-mail address: s.a.j.tas@tudelft.nl (S.A.J. Tas).

https://doi.org/10.1016/j.margeo.2022.106753
Received 23 November 2021; Received in revised form 6 February 2022; Accepted 8 February 2022
Available online 11 February 2022
0025-3227/© 2022 The Author(s). Published by Elsevier B.V. This is an open access article under the CC BY license (http://creativecommons.org/licenses/by/4.0/).

and/or alongshore (Neal et al., 2002; Augustinus, 1980). The landward migration may also end when a new chenier develops seaward of the active chenier (Woodroffe et al., 1983) or in the event of renewed coastal progradation (Augustinus, 1989). Often, relict cheniers can be observed as a series of coast-parallel ridges in the landscape, separated by muddy soil and/or peat, defined as a chenier plain (Russell and Howe, 1935; Otvos and Price, 1979).

Cheniers are also found along the coastline of Demak, a region on the north coast of Central Java (see Fig. 1a, indicated by the red circle) (Winterwerp et al., 2020; Marfai et al., 2016; Tas et al., 2020; van Bijsterveldt et al., 2021). Relict cheniers do not exist in the coastal plain, so this single band of cheniers along the coast is not part of a chenier plain. Even in landscapes that have undergone extreme (antropogenic) changes, relict cheniers are easily distinguishable because of their higher elevation and different composition, generating a sharp contrast to their surroundings. As a result, they are often used for roads, dikes and settlements (Russell and Howe, 1935; Anthony et al., 2011). The existence of a chenier plain can also be seen in deflections in drainage patterns (Otvos and Price, 1979). In the coastal area of Demak, however, all roads, dikes and villages are on lines perpendicular to the coastline, following the embankments of rivers and canals (see Fig. 1b-c).

The mangrove-mud coast of Demak has experienced extreme coastal erosion over the last decades (Ervita and Marfai, 2017); at some locations the coastline has retreated with more than a kilometre (compare Fig. 1b and c). The mangrove forest that used to cover the entire coastal area (Lang, 1869) has been nearly completely converted to aquaculture ponds or cleared for the expansion of the nearby city of Semarang. Furthermore, ground water extraction has caused subsidence up to 20 cm/year in Semarang (Abidin et al., 2013; Kuehn et al., 2010), but also in rural areas subsidence is large enough to drown coastal villages, the vegetated foreshore and mudflats (van Bijsterveldt, 2021). As a result, a large part of the coastal plain is now flooded by tides on a daily basis.

Demak features a tropical monsoon climate, alternating a dry, south-easterly monsoon, usually between April and November, with a wet, north-westerly monsoon. Thanks to the orientation of the coastline in Demak, the south-easterly wind is directed offshore, and results in very calm conditions nearshore. The highest waves occur in the afternoon, when an onshore sea breeze develops locally (Fitrianti et al., 2018).

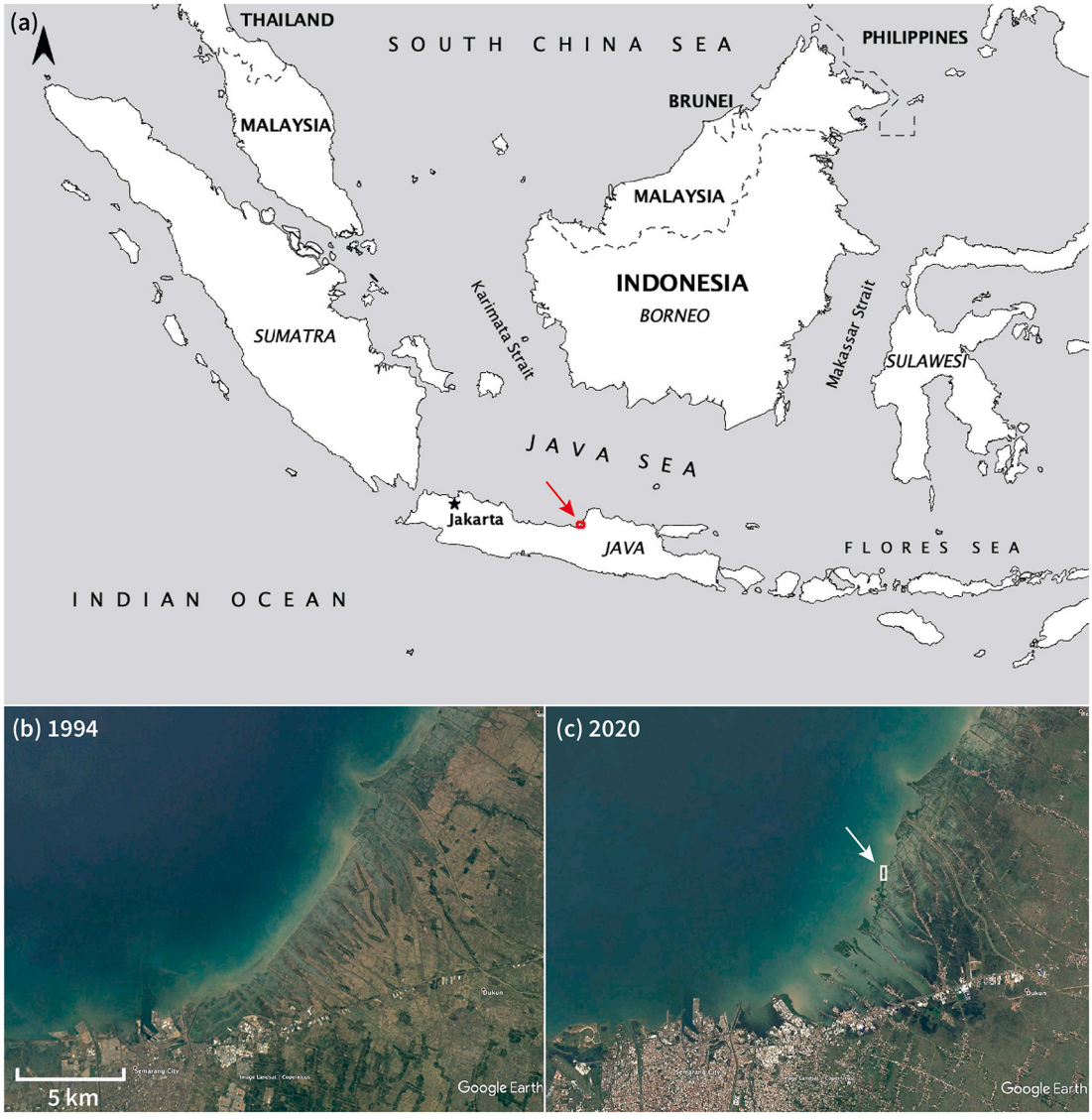

Fig. 1. **(a)** Map of the Java Sea and surroundings. The red dot on the north coast of Central Java indicates the location of the two inset photos shown in **(b)** and **(c)**, which are satellite images of the coastline of Demak in 1994 and 2020 respectively (Google Earth, 2021). They highlight the extreme coastal erosion and coastline retreat in this area, as well as the rapid development of Semarang in the south. The white rectangle in **(c)** indicates the location of the zoomed satellite images in Fig. 2a-d. (For interpretation of the references to colour in this figure legend, the reader is referred to the web version of this article.)

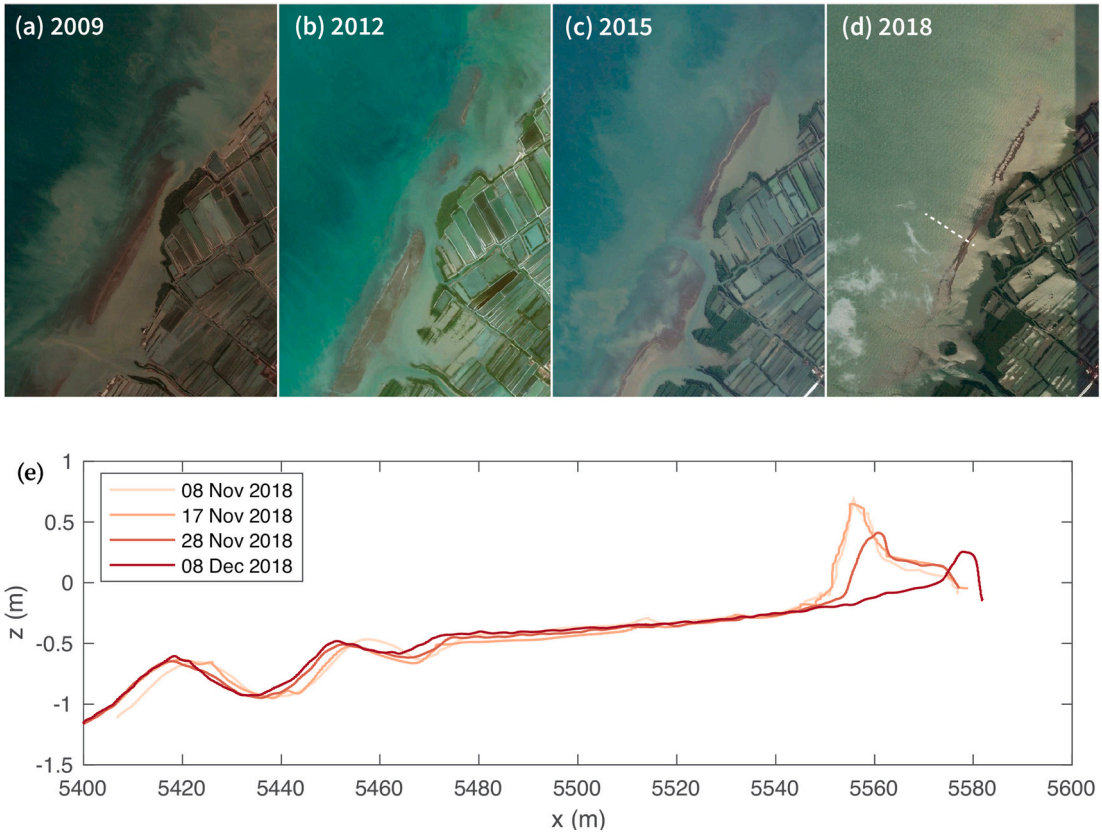

Fig. 2. Google Earth images (Google Earth, 2021) showing the position of a chenier in **(a)** 2009, **(b)** 2012, **(c)** 2015 and **(d)** 2018 (see the white rectangle in Fig. 1c for the location of this chenier along the coast of Demak). The profiles in **(e)** were measured with a Differential Global Positioning System (DGPS) between 8 November 2018 (light red line) and 8 December 2018 (dark red line). The white dashed line in **(d)** indicates the transect along which the profiles in **(e)** were measured. (For interpretation of the references to colour in this figure legend, the reader is referred to the web version of this article.)

Waves are generally higher during the onshore-directed NW monsoon, but during this period also storms occasionally occur. The tide can be characterised as micro-tidal with a maximum tidal range of around 1 m and it is mixed, mainly diurnal (based on water level time series measured between May 2016 and December 2018 in Semarang (Flanders Marine Institute (VLIZ) and Intergovernmental Oceanographic Commission (IOC), 2021)).

The cheniers in Demak are not only unique in their absence of a chenier plain, but also for their cross-shore dynamics. In other locations around the world, the cross-shore migration of cheniers is largely in the landward direction (Augustinus, 1989; Otvos, 2019; Quaresma et al., 2007) with migration rates usually decreasing over time because as the chenier moves higher, overwash becomes less frequent. For example, both in Saemangum, Korea and Mont-Saint-Michel Bay, France initially an onshore migration speed of 50 m/y was reported, which later reduced to 5 m/y in Korea (Kim et al., 2020) and 1–2 m/y in France (Weill et al., 2012). The highest onshore migration rates were reported on the Saltés Island chenier plain in Spain, up to 675 m in 3 years, averaging 225 m/y (Morales et al., 2014). Woodroffe et al. (1983) recorded onshore migration of 10 m within a week, due to a storm event. Brunier et al. (2019) measured onshore migration rates of cheniers over coastlines that were rapidly retreating as a result of mangrove removal and fragmentation due to urbanisation and farming (very similar to the situation in Demak), and these rates were much higher than in areas with a healthy mangrove coastline (up to 70 m in 6 months). However, satellite images of Demak between 2009 and 2018 (see Fig. 2a-d) reveal that the chenier remained more or less at the same location over a period of 10 years. However, on shorter timescales the chenier is very dynamic, moving landward up to 8 m/day (see Fig. 2e and Tas et al. (2020)).

The aim of this paper is to understand the drivers of cross-shore chenier dynamics during their 'active phase', i.e. the phase between their formation and the moment the chenier is stranded on the shoreline and no longer mobile in response to daily wave and tidal influences. Whereas cheniers described in literature have one primary migration mode (landward migration until stranded), observations of the chenier in Demak suggest that there may be an alternative stable state where a chenier is very dynamic on the short term, but still maintains an equilibrium position (not attached to the coastline) over longer timescales. This implies that there is also a mechanism that transports the chenier offshore. To better understand the short-term and long-term dynamics and underlying transport mechanisms, we have constructed an idealised morphodynamic chenier model. The set-up of this model is described in Section 2. In Section 3, we calibrate the model results with (short term) field measurements, and then address the chenier response to various boundary conditions. In Section 4 we compare the model results to observed chenier dynamics in literature, assess the specific dynamics in Demak, draw an analogy between breaker bars and cheniers, and discuss how cheniers could be part of a negative feedback loop induced by the erosion of a drowning coastal plain.

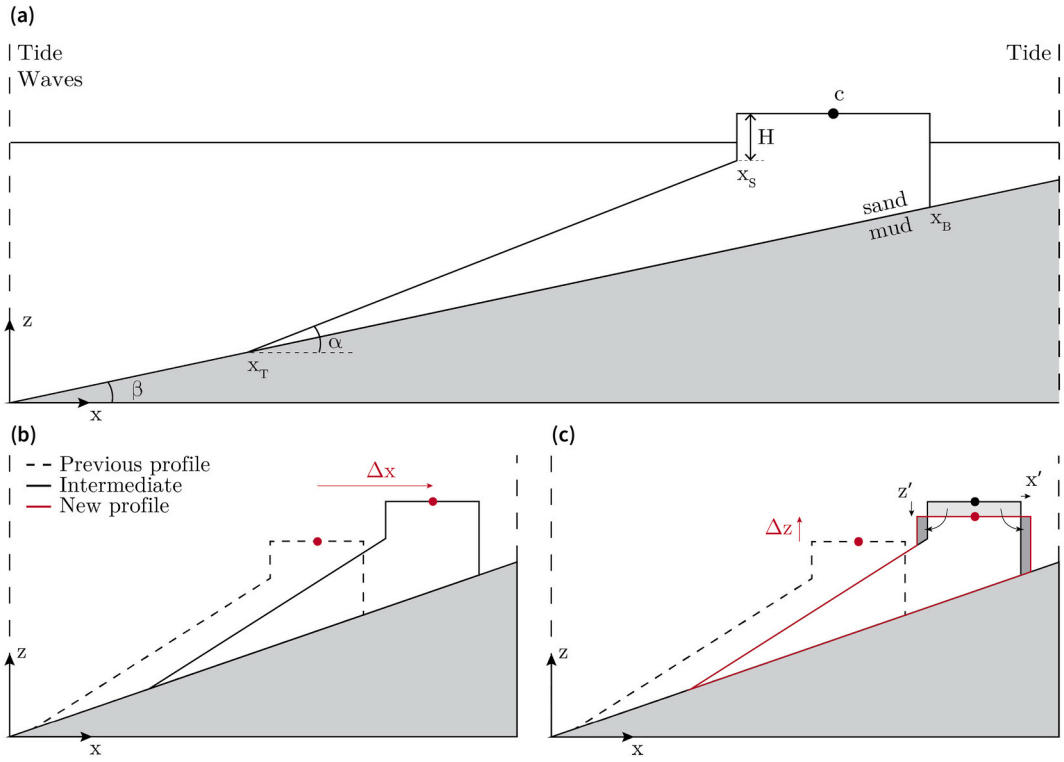

Fig. 3. **(a)** Idealised chenier geometry, defined by the chenier toe (x_T), the beachface toe (x_S), the toe of the back-barrier face (x_B) and the chenier crest height (H). The chenier center (C) is indicated with a dot. The chenier body is composed of sand (white) and lies on top of a muddy substrate (gray). The muddy shoreface has a slope of β, and the chenier slope has a steeper slope of α. The chenier evolution is explained in two steps: **(b)** first the entire chenier unit is moved horizontally with Δx along the muddy substrate; **(c)** then the vertical change is corrected with z' such that the total vertical change equals Δz. This vertical correction yields a change in width with x' on both sides in order to conserve the volume/surface area of the chenier.

2. Methods

A wide range of morphological models exists in literature, ranging from high complexity numerical models to a simple set of empirical equations. High complexity models often account for most of the relevant transport processes, but they also have several disadvantages. Computational times are often long, it is not straightforward to differentiate underlying processes, and imperfect descriptions of the physics may lead to unrealistic model behaviour (such as the predictions of nearshore sandbar dynamics; see Cohn et al. (2019); Dubarbier et al. (2015); Spaans (2019)). Idealised models are specifically designed to focus on processes that are considered essential to describe a particular phenomenon. Idealised models are fast and suitable to investigate certain processes, but lack the complex physics of numerical models. When selecting a modelling approach, the most appropriate scales (temporal and spatial) of the system need to be determined. Observations of the chenier system in Demak (see Fig. 2) have shown that a large range of timescales is required: from the short-term dynamics, to the long-term (average) stability. Besides resolving the appropriate scales, the selected modelling approach should be computationally feasible, have a sound physical basis and demonstrate useful predictive skill (French et al., 2016).

In this section we will present a hybrid model, which is essentially an idealised model coupled to a complex numerical model. The numerical model provides the sound physical basis on short time scales (role of waves and tides in sediment transport and morphology), which is synthesised in a look-up table. The idealised model is inspired by the elegant barrier model of Lorenzo-Trueba and Ashton (2014), and computes long-term chenier morphodynamics for a range of scenarios using the look-up table generated by the numerical model. This hybrid approach allows for a very low computational effort. The model is applied in exploratory mode (Murray, 2003), i.e. to investigate the role of specific processes, so not to reproduce a specific development in great detail.

2.1. Chenier geometry

We approximate the cross-sectional dynamics of the chenier with an idealised geometry, similar to idealised geometries of deltas and barrier islands (Parker and Muto, 2003; Lorenzo-Trueba and Ashton, 2014), see Fig. 3a. The model consists of two components: the muddy subsurface, and the sandy chenier. We assume the muddy substrate to be static; it has a constant slope of β and there is no sediment exchange between the two components. The chenier body is defined by four parameters: the chenier toe (indicated with subscript T), the beachface toe (subscript S), the toe of the back-barrier face (subscript B) and the height of the chenier crest (H, defined as the vertical distance between the beachface toe and the crest of the chenier). The model assumes conservation of sand volume, so the surface area defined by these four parameters in the cross-section remains constant. The surface area/volume of the chenier is represented by one single point in the computations: the chenier center (subscript C). This point is defined horizontally as the middle

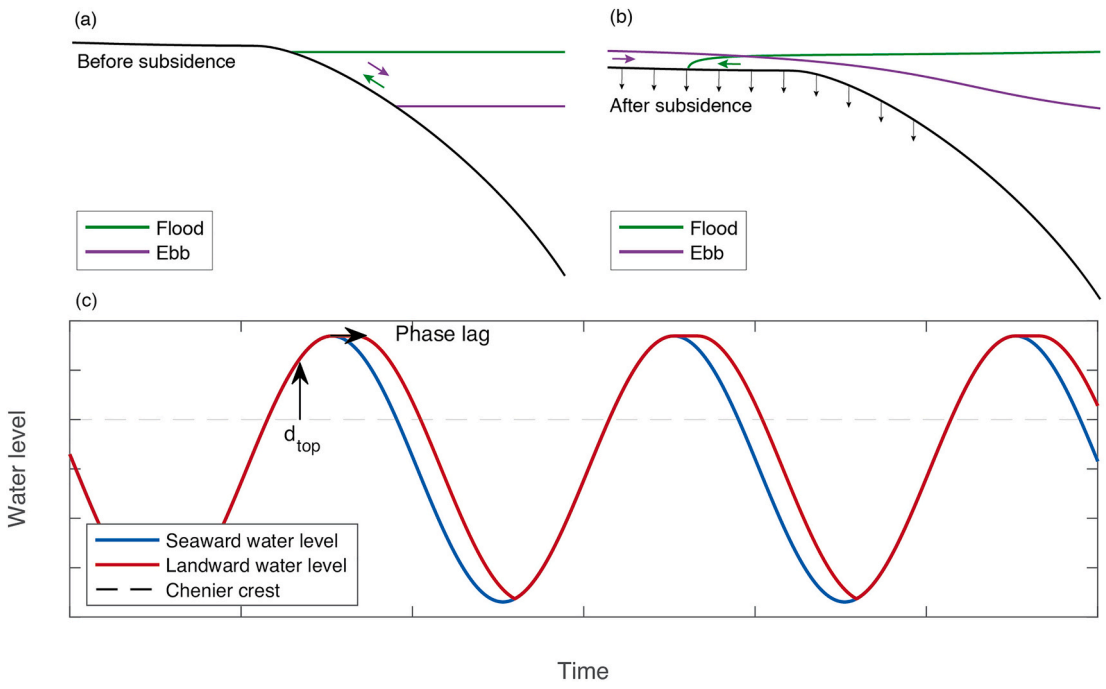

Fig. 4. **(a)** Situation without a drowned hinterland due to subsidence: no phase lag. **(b)** Situation where subsidence has caused the hinterland to flood with each high tide (green line), which causes a phase lag to develop during ebb (purple line); water levels are vertically exaggerated for illustrative purposes. **(c)** Water level time series applied to the seaward model boundary (blue line) and landward model boundary (red line). During flood both water levels are in phase, during ebb the landward water level lags behind. (For interpretation of the references to colour in this figure legend, the reader is referred to the web version of this article.)

between the beachface and the back-barrier face, $x_C = x_S + (x_B - x_S)/2$, and vertically as the highest point of the chenier, $z_C = z_S + H$. The chenier toe has a slope α, which is steeper than the offshore shoreface slope β. The slope of the beach and back-barrier is several orders of magnitude steeper (Heward, 1981) and are approximated as vertical.

2.2. Chenier dynamics

The idealised chenier evolves over time by prescribing hourly displacement rates, computed with a process-based model (Delft3D), which will be specified in more detail in the section hereafter. Every hour, the chenier center moves horizontally with Δx and vertically with Δz (derived from Delft3D for the specific boundary conditions at that time step), and the shape of the chenier (height and width) changes such that the total volume of sand remains constant. This procedure is explained in two steps and is illustrated in Fig. 3b-c: first, the entire chenier migrates upslope (or downslope if $\Delta x < 0$), without changing the shape of the chenier (see Fig. 3b). Since the muddy substrate has a slope β, this horizontal migration with Δx automatically yields a vertical change as well, equal to $\beta\Delta x$. However, this vertical change is not necessarily equal to the total vertical change of the chenier center, Δz. Therefore, the vertical change needs to be corrected with z' such that the total vertical change of the chenier center equals $\Delta z = \beta\Delta x - z'$ (see Fig. 3c). In case $\Delta z < \beta\Delta x$, sediment is removed from the crest of the chenier, and equally distributed on both sides in terms of lateral expansion x' (so that the horizontal position of the chenier center is maintained). In case $\Delta z > \beta\Delta x$, the crest of the chenier is heightened with sediment from both sides of the chenier crest, reducing the width of the chenier with $2x'$ and increasing the height of the chenier H with z'.

The new coordinates of the four chenier parameters (subscript 1) can be expressed in function of Δx, Δz, and the coordinates at the previous time step (subscript 0):

$$x_{T,1} = x_{T,0} + \Delta x, \tag{1}$$

$$z_{T,1} = z_{T,0} + \beta\Delta x, \tag{2}$$

$$x_{S,1} = x_{S,0} + \Delta x - x', \tag{3}$$

$$z_{S,1} = z_{S,0} + \beta\Delta x - \alpha x', \tag{4}$$

$$x_{B,1} = x_{B,0} + \Delta x + x', \tag{5}$$

$$z_{B,1} = z_{B,0} + \beta\Delta x + \beta x', \tag{6}$$

$$H_1 = H_0 - \beta\Delta x + \Delta z; \tag{7}$$

where

$$x' = \frac{(x_{B,0} - x_{S,0})(\beta\Delta x - \Delta z)}{2H_0 + 2\Delta z + z_{S,0} - z_{B,0} - \beta\Delta x}. \tag{8}$$

For all steps in the model described above, sediment mass is conserved (i.e. the total body of sand in the chenier does not change in time). The horizontal and vertical displacements, Δx and Δz are a function of (1) the offshore wave height, $H_{s,\infty}$; (2) the water depth on top of the chenier crest, d_{top} (see Fig. 4c); (3) the phase of the tide (ebb or flood); and (4) a phase lag, θ (see Fig. 4c). We use a process-based model to determine the relationship between Δx and Δz on one hand, and the

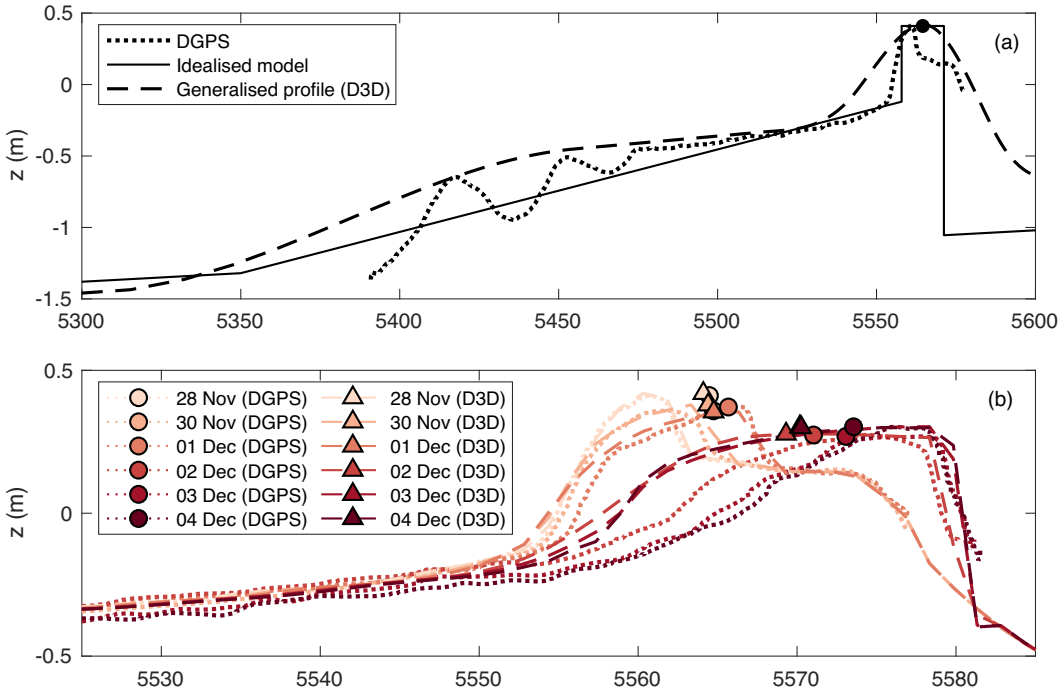

Fig. 5. **(a)** Bathymetric profile measured with a DGPS in Demak, Indonesia (dotted line), with its representative idealised geometry (solid line) and a generalised chenier profile for the Delft3D simulations (dashed line). The chenier center of all three profiles coincides and is indicated with a dot. **(b)** Comparison of the validation run with Delft3D (dashed lines) to the measured profiles (dotted lines). The colours represent the days between 28 November 2018 and 4 December 2018. The chenier center of the measured profiles is indicated with a dot, and a triangle for the Delft3D profiles.

tidal and wave conditions on the other hand, through a large number of model realisations. Before introducing this process-based model, we first elaborate on the the phase lag θ.

2.3. Boundary conditions

The chenier only becomes mobile when it is fully submerged,[1] i.e. when the water level η exceeds the chenier crest level $\eta > z_S + H$. Field observations (Tas et al., 2020) showed that both tide and waves are responsible for sediment transport on the cheniers of Demak. Waves transport sediment directly, through skewness, and indirectly, through stirring, where waves stir up the sediment which is then transported by tidal currents. Tidal currents are only sufficiently strong to resuspend sediments when the water depth above the chenier is very small. Most sediment transport occurs when high tide (i.e. inundated chenier) coincides with high wave events. Weill et al. (2012), for instance, showed that most chenier migration took place when the 4.4-year and/or 18.6-year tidal cycles caused higher water levels in the Mont-Saint-Michel Bay, while Tas et al. (2020) linked chenier migration to the interaction between the diurnal component of the tide and the sea breeze-induced waves which occurred in the afternoon.

Due to coastal erosion and subsidence, large parts of the coastal plain in Demak flood during each tide. This drowning of the coastal plain induces a phase lag in tidal flow over the chenier. Due to the strong antropogenic influence in this area, this phase lag is even more pronounced than in undisturbed systems, for the following reasons. The drowned coastal plain is characterised by a few channels (either remnants of man-made channels, or naturally formed creeks) with relatively low hydraulic drag (Bayliss-Smith et al., 1979; Friedrichs, 2010), while the rest of the basin is covered by obstacles (such as mangrove vegetation, aquaculture pond bunds, houses etc.) which generate high friction (Temmerman et al., 2005; Horstman et al., 2013, 2021). The rising tide can enter the tidal basin through the channels, eventually flooding the entire area; during ebb the water flows back first over the high-friction shallow areas, before reaching the channels and creeks (Friedrichs and Madsen, 1992; Mazda et al., 1995; Horstman et al., 2021). Due to the high resistance, this ebb flow is slowed down, and a tidal phase lag develops between the tidal basin and the open sea. Lower friction in the straight, man-made channels and higher friction on the tidal flats due to remnants of constructions creates an even larger phase lag. This phase lag generates a cross-shore water level gradient near the mouth of the channels and creeks. When a (sufficiently long) chenier is present in front of a channel mouth, this water level gradient occurs over the chenier crest, resulting in a residual seaward-directed flow. The magnitude of this flow (and the resulting sediment transport) is related to the tidal range and inversely related to the water depth above the chenier crest.

This results in three boundary conditions for the idealised chenier model: an offshore wave height, applied at the seaward boundary, and two water levels, one applied at the seaward boundary and one at the landward boundary. During flood, these water levels are in phase, while during ebb a phase lag may be prescribed at the landward boundary, see Fig. 4.

2.4. Process-based model

The values of Δx and Δz used in the idealised model are computed using a morphodynamic model set-up in Delft3D. Delft3D is a process-based modelling suite that is capable of simulating hydrodynamics (flow and waves), sediment transport and morphology (Lesser et al., 2004). This Delft3D model set-up uses an alongshore uniform, generalised profile representative for a chenier (dashed line in Fig. 5a). Similar to the idealised geometry, the chenier center of this generalised profile in D3D is defined as the part of the chenier above the lowest low water

[1] In reality this is less straightforward: while the mean water level may be below the chenier crest level, higher waves could roll over the crest and transport sediment. To account for this transport, the water level in the model is increased with 10% of the significant wave height.

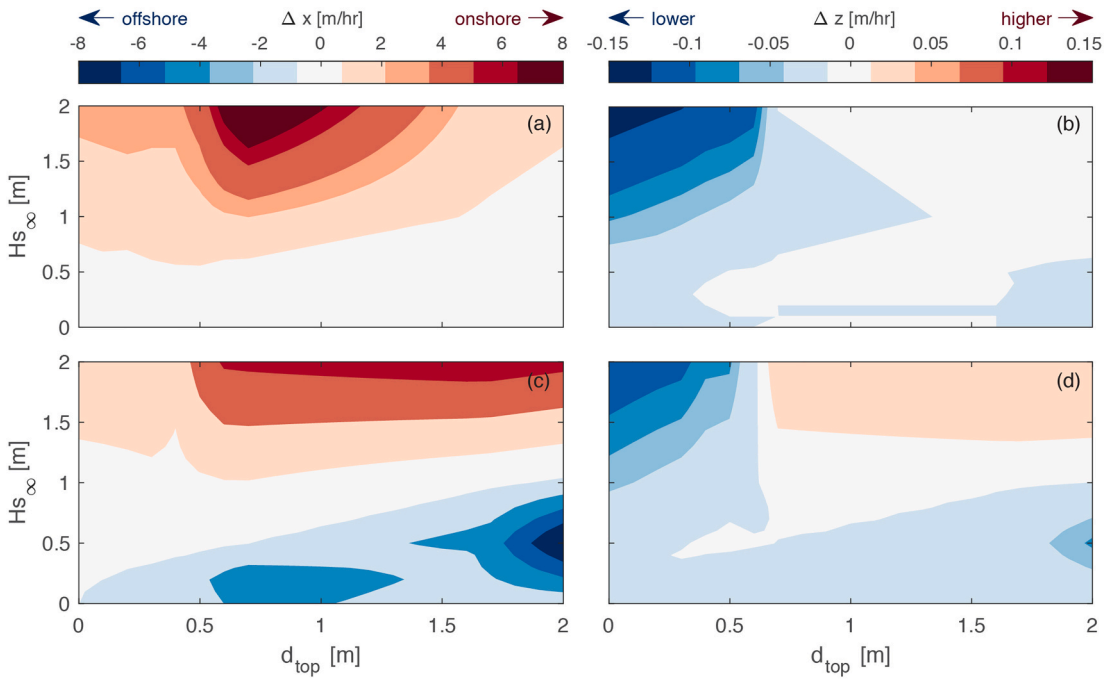

Fig. 6. Hourly horizontal and vertical displacement based on the Delft3D model for some of the scenarios. The left column (**(a)** and **(c)**) shows the values of Δx and the right column (**(b)** and **(d)**) Δz; while the upper row (**(a)** and **(b)**) shows the displacements for a situation during ebb without a phase lag ($\theta = 0$ min) and the lower row (**(c)** and **(d)**)a situation during ebb with a phase lag of $\theta = 10$ min. Within the contour plot, the horizontal axis shows the water depth on top of the chenier d_{top} and the vertical axis the deep water wave height $H_{s,\infty}$. The red colour represents an onshore or upward shift for Δx and Δz respectively, blue means offshore-directed (Δx) or lowering (Δz). (For interpretation of the references to colour in this figure legend, the reader is referred to the web version of this article.)

line. The chenier center of the generalised profile used in Delft3D has the same coordinates as the center of the idealised geometry used in the idealised model (solid line in Fig. 5a).

At the seaward boundary of the Delft3D domain, a time-varying water level and wave height is prescribed. The wave height is the wave height at deep water, corrected for shoaling to the water depth at the model domain boundary. The landward end of the domain is also an open boundary, where only a water level time series is prescribed (to which the phase lag θ applies).

The Delft3D model is run for a representative range of calm to moderate conditions, representative for the SE monsoon season: (1) $H_{s,\infty} = 0 - 2$ m; (2) $d_{top} = 0 - 2$ m; (3) ebb or flood; and (4) $\theta = 0 - 20$ min.

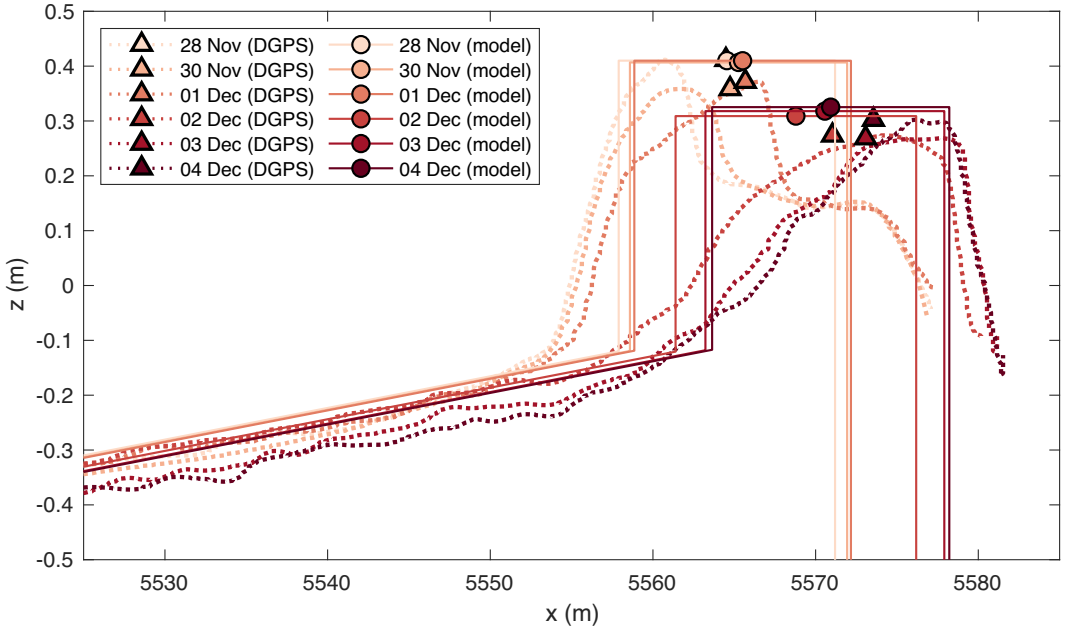

Fig. 7. Comparison of the idealised model (solid lines) with measured profile changes (dotted lines). The chenier center in the idealised model profiles is indicated with a dot and in the computed model profiles with a triangle.

Since measurements were collected during the SE monsoon season, the model can only be validated for calm to moderate conditions (see Section 2.5), and therefore storm conditions are not considered here. For each possible combination of boundary conditions, the model is run for 6 h, and the bed level change between the second and sixth hour of the model simulation is used to determine the average change per hour (so total change divided by 4 h). These values are stored in an hourly displacement matrix (see Fig. 6). For each time step in the idealised chenier model, the values of Δx and Δz are interpolated for the current values of $H_{s,\infty}$, d_{top}, ebb/flood, and θ from the displacement matrix.

Fig. 6 visualises the different hourly displacements for a range of water depths above the chenier (horizontal axis) and offshore wave heights (vertical axis). The left panels (a and c) show the hourly horizontal displacement Δx in m, where blue colours represent offshore migration and red colours onshore migration; the right panels (b and d) show the hourly vertical displacement Δz in m, where blue colours represent lowering of the chenier crest and red colours heightening. The first row (a and b) shows a scenario during ebb when there is no phase lag; the second row (c and d) shows a scenario during ebb with a phase lag $\theta = 10$ min.

From Fig. 6a we can derive that higher waves lead to more onshore transport, and combined with Fig. 6b, higher waves also lead to a lowering of the chenier crest for small water depths. The absence of blue shades in Fig. 6a reveals that under these circumstances, the chenier only migrates onshore. Only when introducing a phase lag during ebb (Fig. 6c-d), the chenier also migrates in the offshore direction (for smaller wave heights in combination with larger water depths).

2.5. Validation Delft3D model

The Delft3D model was validated with 6 days of data collected at a chenier off the mangrove-mud coast in Demak, Indonesia between 28 November 2018 and 4 December 2018. The measured initial profile (dotted line in Fig. 5a) is used as initial profile for this validation run. For the validation run, offshore waves were measured with a WaveDroid directional wave buoy and water levels were measured with two OSSI-010-003C-01 Wave Loggers, one which was deployed seaward of the chenier and one landward. The profiles computed with Delft3D (dashed lines, triangle for chenier center) are shown in Fig. 5b and compared to the measured profiles (dotted lines, dot for chenier center). While the exact shape of the profiles diverges slightly over time, the migration of the chenier center of both the measured and modelled profiles remain very similar.

3. Results

3.1. Calibration idealised chenier model

The first set of model results with the idealised model (not shown here) predicted a gradual lowering of the chenier crest. This lowering results from the tendency that morphodynamic models such as Delft3D tend to flatten bars (van Duin et al., 2004). We mitigate this shortcoming through a vertical correction z_{corr}, so that the Δz applied in eqs. 3–7 becomes $\Delta z = \Delta z_{D3D} + z_{corr}$. The value of z_{corr} was calibrated using the measured profiles. Various distributions were tested, but in the end the most optimal results were obtained for a constant value of $z_{corr} = 0.0015$ m/h. The resulting profiles computed with the idealised model simulation are shown in Fig. 7 (solid lines) and compared to the measured profiles (dotted lines).

While the modelled profiles may not perfectly follow the measured profiles, the trends are very similar: small changes the first days, followed by a larger landward migration and lowering, and on the last days small horizontal migration accompanied by some heightening of the crest.

3.2. Idealised boundary conditions

As a next step, the model is run for a much longer time span of 10 years. These longer model simulations are first executed with a schematic, idealised set of boundary conditions. A water level time series is constructed with the two main tidal constituents in Demak: K1 and M2. Based on the typical sea-breeze induced waves, a schematic wave time series is constructed, with waves during the afternoon and evening only (between 14 h00 and 22 h00), while the rest of the day no waves occur (since the SE monsoon wind is directed offshore, resulting in very calm conditions nearshore). During the sea breeze, the wave height is constant, $H_{s,\infty} = 0.23$ m, representative for the waves measured with a WaveDroid at deep water during sea breeze events. Fig. 8 shows the

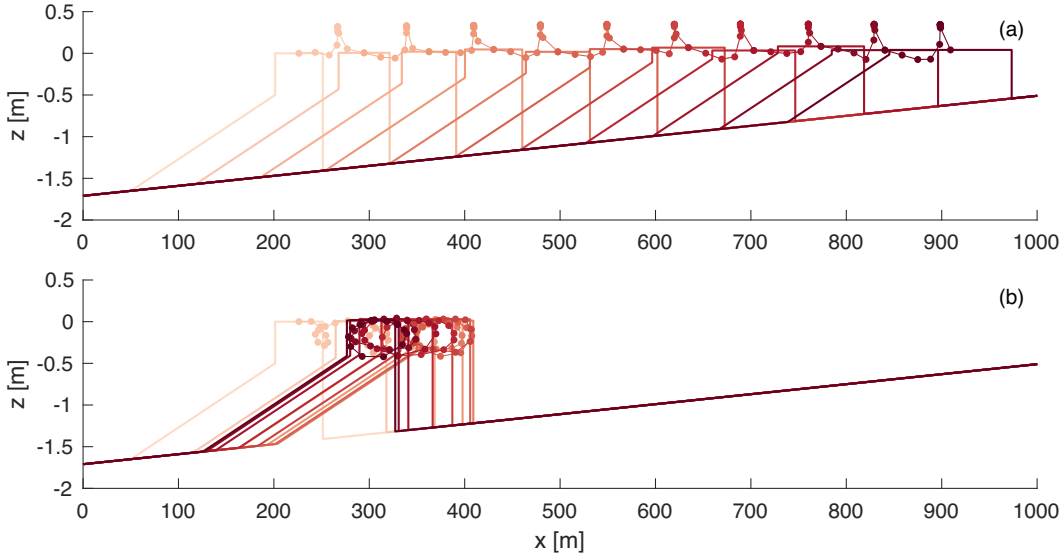

Fig. 8. Chenier evolution under idealised boundary conditions, for a situation **(a)** without phase lag, and **(b)** with a phase lag of $\theta = 3.5$ min. One profile per year is shown, with increasingly darker shades of red over time. The chenier center is indicated with a dot, and is shown for each month, giving an impression of the dynamics during the year. (For interpretation of the references to colour in this figure legend, the reader is referred to the web version of this article.)

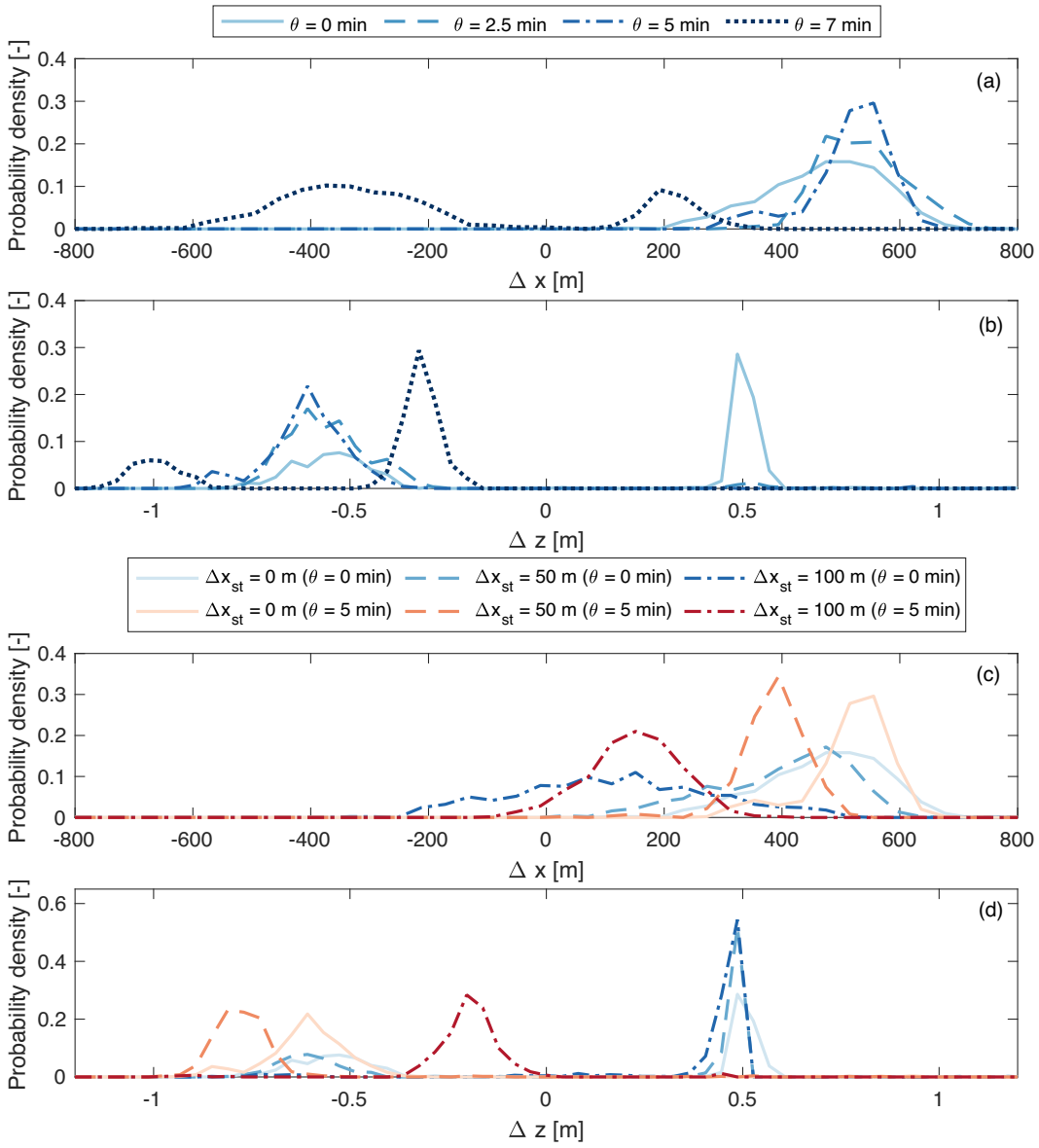

Fig. 9. Probability density functions of the horizontal (**(a)** and **(c)**) and vertical (**(b)** and **(d)**) displacement (relative to the initial position) for different scenarios over a period of 10 years after 500 realisations. The effect of different phase lags is shown in **(a)** and **(b)**, with increasingly darker shades of blue (and going from solid via dashed, dash-dotted to dotted lines) for larger values of the phase lag, θ. The effect of a storm reset Δx_{st} is visualised in **(c)** and **(d)**, with increasingly darker shades for larger values of Δx_{st}. Blue lines represent a situation without a phase lag; red lines $\theta = 5$ min. (For interpretation of the references to colour in this figure legend, the reader is referred to the web version of this article.)

resulting profiles after 10 years as a result of these schematic boundary conditions, both without a phase lag ($\theta = 0$, Fig. 8a), and with a phase lag ($\theta = 3.5$ minutes; Fig. 8b).

For the scenario without phase lag (Fig. 8a), the chenier migrates onshore. Interestingly, this migration rate is not constant throughout the year. For a couple of months, the chenier migrates rather rapidly onshore, generally accompanied by a small lowering of the crest level. This onshore migration is halted rather abruptly, and replaced by a strong vertical growth, until the chenier has reached a height close to high water level. It remains stable for a while, until at some point the maximum water levels are high enough to submerge the chenier. The chenier crest then lowers rapidly and the chenier again migrates rapidly onshore starting a new cycle that is repetitive over multiple years. This cyclic pattern is a result of the timing between the sea breeze-induced waves and the tide. The sea breeze always occurs at exactly the same time (during the afternoon, between 14 h00 and 22 h00), but the time of the (diurnal) high tide shifts a day in a year (see Fig. 9 in Tas et al. (2020)).

The persistent wave-driven onshore migration in Fig. 8a) result in onshore welding of the chenier, and not in a dynamically stable chenier as observed in Demak. This stability does result from a non-zero phase lag (Fig. 8b). The phase lag (see Section 2.3) creates a water level

gradient over the chenier, with higher water levels on the landward side. This induces flow over the chenier in offshore direction, driving offshore sediment transport. For values of θ close to $\theta = 3.5$ min (and a sea breeze-induced wave height of $H_{s,\infty} = 0.23$ m), the onshore migration by waves is balanced by the offshore migration during ebb induced by the phase lag. As the timing between the sea breeze-induced waves and the tide shifts, one process becomes dominant over the other, resulting in a circular pattern over the year. This balance only occurs for a very small range of combinations of wave height and phase lag; for all other combinations the chenier either migrates onshore or offshore.

3.3. Stochastic boundary conditions

In the previous section, the boundary conditions were reduced to a set of idealised conditions to identify the role of moderate wave conditions and θ. In reality, the boundary conditions are much more variable. The tide consists of a wide range of constituents, and while the pattern of the sea breeze is fairly regular, its magnitude and presence may vary. To account for these variations, the model is forced with water levels computed with a full set of tidal constituents, and a stochastic wave climate based on measurements collected with a WaveDroid during August 2017, April 2018 and October–November 2018 (all during the SE monsoon season). The corresponding time series is constructed as follows.

Field observations show that a sea breeze occurred for 50% of time. The synthetic wave conditions time series is thus determined in two steps: first, the occurrence of a sea breeze (hence, whether there are waves in the afternoon) is determined randomly with a 50% probability of sea breeze. Then, if there is a sea breeze that day, a wave height is randomly picked from a database containing observed daily wave heights. For the first and last hour of the sea breeze event (14 h00 and 22 h00), the wave height is 50% of the representative wave height, the other six hours the wave height is 100% of the representative wave height to mimic the onset and waning of the sea breeze.

The random selection of wave input parameters allows for a stochastic evaluation of chenier dynamics by creating many realisations (500 in this case), generating a probability density function (pdf) of horizontal and vertical chenier displacement for various scenarios. The pdfs computed with four different values of θ (0, 2.5, 5 and 7 min; Fig. 9a-b) reveal that for the situation without a phase lag (lightest shade blue, solid line), the horizontal and vertical migration is positive (i.e. the chenier migrates onshore and the crest level becomes higher).

For small phase lags, the chenier still migrates onshore (positive horizontal migration), but the crest level lowers (negative vertical migration). This vertical migration is accompanied by a widening of the crest, i.e. the chenier spreads out to become an increasingly thinner layer of sand on top of the muddy substrate. Moreover, the lowering of the crest is limited by the stable muddy substrate (which is a consequence of our assumption of a constant slope), so when the crest level reaches the muddy substrate, the chenier is assumed to have dissolved.[2] For $\theta = 2.5$ min, 95% of the model realisations reach this point within 10 years, with an average simulation time of 3.6 years. For $\theta = 5$ min, 98% of the model realisations reach this point within 10 years, with an average simulation time of 2.5 years. In other words, for small phase lags, the chenier dissolves as a wide, fine layer of sand on top of the muddy substrate. This layer of sand is located closer the shoreline for smaller phase lags.

For larger phase lags, such as $\theta = 7$ min (darkest blue, dotted line in Fig. 9a-b), the chenier migrates in offshore direction (with its crest just below MSL). As can be seen by the double peak in the pdfs, part of the simulations (around 25% of the model realisations) shows the same behaviour as for the smaller phase lags, with the chenier migrating onshore while lowering until the chenier sand spreads out over the muddy substrate and the chenier dissolves (although this fine layer of sand is further offshore compared to a situation with a smaller phase lag).

Similar to the idealised boundary conditions, the chenier remains stable horizontally for only a narrow range of phase lags θ. Smaller values lead to onshore migration until either the crest reaches high tide, or the crest lowers until the chenier dissolves as a wide, thin layer of sand on the muddy substrate closer to the shoreline. Larger values lead to offshore migration, with the crest between low tide and MSL.

While the phase lag mainly has a horizontal effect (onshore vs. offshore migration), it also has a small vertical effect (generally two orders of magnitude smaller than the horizontal displacement, see Figs. 6 and A.12). This vertical effect can cause an indirect horizontal effect, because by lowering the crest, the chenier is submerged longer, which in turn may lead to additional horizontal displacement. In some cases, it is therefore possible that a scenario with a phase lag may lead to more onshore migration than a scenario without a phase lag (compare the tails of the pdfs of $\theta = 0$ min and $\theta = 2.5$ min in Fig. 9a).

The model realisations in Fig. 9a-b assume a year-round dominance of sea-breeze conditions (as this was the period for which we had data available). However, these conditions are only representative for the SE monsoon season. Between December and March (the NW monsoon season) winds are constantly onshore, resulting in higher waves throughout the entire day, and with occasional storms. Due to the absence of measurements during the NW monsoon season, the idealised chenier model has not been tested and calibrated for such conditions. Moreover, there are no satellite images available during these months due to cloud cover. However, comparing the last satellite image before the NW monsoon season with the first image after, suggests that there is a net offshore migration over the NW monsoon season. To avoid using the model under storm conditions (for which we do not have field data to calibrate the model with, moreover during storm conditions other processes may govern the chenier dynamics) we simplify the net effect of the storm season as a net seaward displacement over a distance Δx_{st} at the last time step of the SE monsoon season. This new position is then the starting point for the calculations of the next SE monsoon season. The exact magnitude of such a storm reset is unknown; based on Google Earth images, it is estimated to be in the order of 50 m. However, cloud cover typical for the NW monsoon season prevent an accurate estimate for Δx_{st}. Therefore, $\Delta x_{st} = 50$ m and $\Delta x_{st} = 100$ m are both tested and compared to $\Delta x_{st} = 0$ m to assess the effect of this storm reset.

Fig. 9c-d shows the probability density functions of the horizontal and vertical displacements after 10 years, for different values of Δx_{st} (darker colours for larger storm resets) and with (red colours) and without (blue colours) phase lag. Without a phase lag, regardless of the magnitude of the storm reset Δx_{st}, the horizontal distribution is wide, but vertically very narrow. This indicates that all simulations converge to a crest around high tide, but there is quite some variation in the amount of horizontal migration. In the case of $\Delta x_{st} = 0$ m (lightest blue shade), the chenier shows the most onshore migration. For $\Delta x_{st} = 50$ m, the chenier still migrates onshore, but less; for $\Delta x_{st} = 100$ m the horizontal migration is smallest, and could be both in onshore or offshore direction. For even larger values of Δx_{st} (not shown), all horizontal migration is offshore-directed.

In the scenarios with a moderate phase lag of $\theta = 5$ min, the chenier crest no longer reaches high tide (as described above). The simulations with a moderate storm reset ($\Delta x_{st} = 50$ m) follow the same behaviour as the scenario without a storm reset, for most model realisations (97%) the chenier sand spreads out as a thin layer on top of the muddy substrate close to shore (average simulation time 5.1 years). However, due to the storm reset, this sand layer is located more seaward than the previous scenario without a storm reset. A larger storm reset ($\Delta x_{st} = 100$ m) does not follow this trend of onshore migration and diffusion over the muddy substrate; instead the chenier remains between MSL and low tide. The horizontal migration remains limited and could be either onshore or

[2] The sand is still present in the system, so at a later point a new chenier may be formed, but that is beyond the scope of this model.

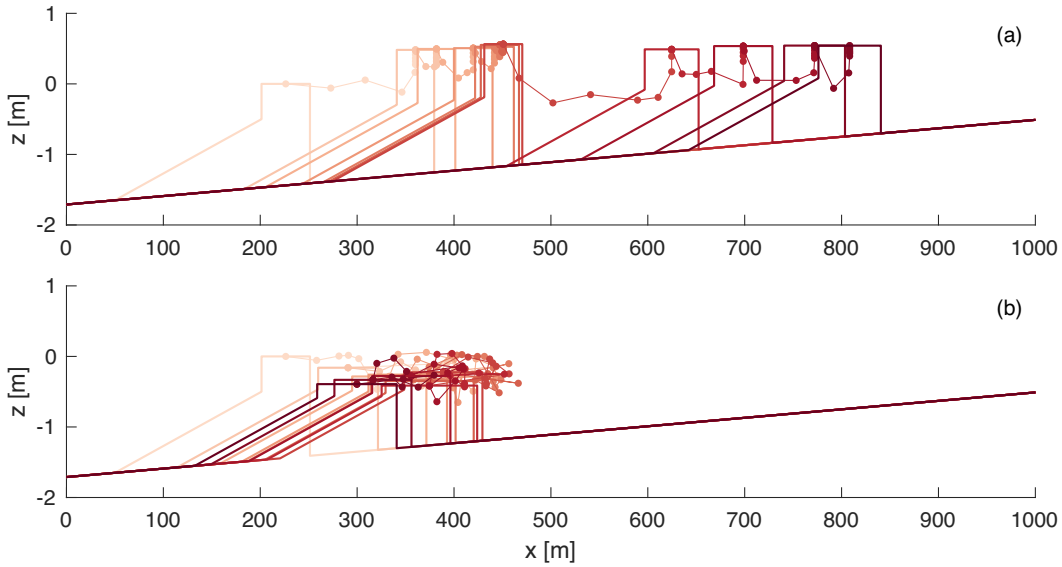

Fig. 10. Chenier evolution over 10 years, under stochastic boundary conditions. One profile per year is pictured, in increasingly darker shades of red. The position of the chenier center is indicated with a dot for each month. Panel **(a)** shows a scenario without phase lag ($\theta = 0$ min) or storm reset ($\Delta x_{st} = 0$ m). Panel **(b)** shows a scenario with a phase lag of $\theta = 5$ min and a storm reset of $\Delta x_{st} = 100$ m. (For interpretation of the references to colour in this figure legend, the reader is referred to the web version of this article.)

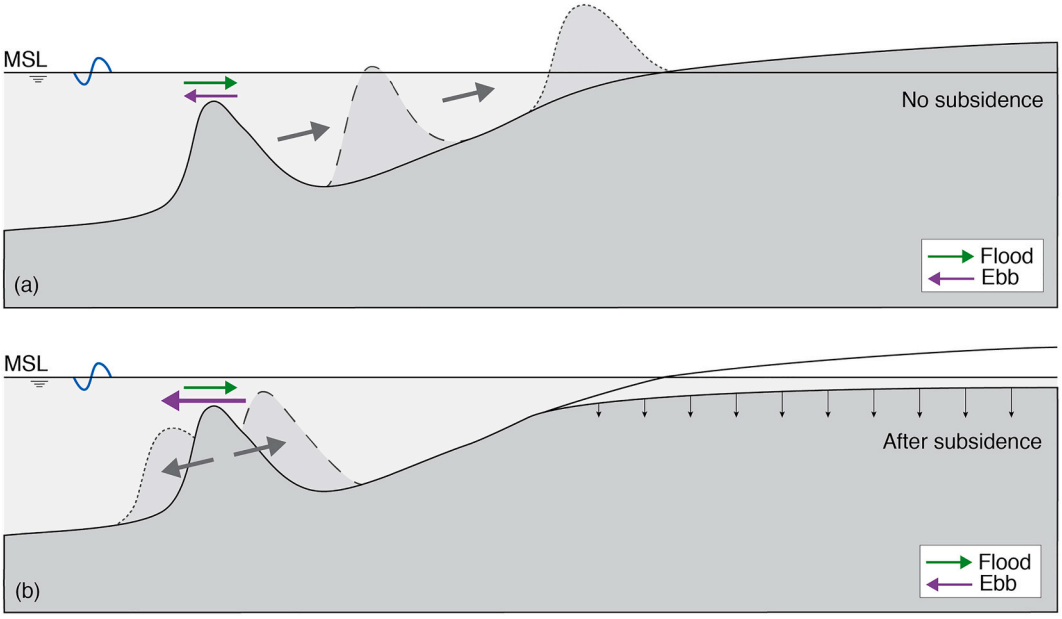

Fig. 11. Conceptual figure summarising the findings of the idealised chenier model. **(a)** shows a coastline without phase lag, where the chenier only migrates onshore under wave action. **(b)** shows the situation off a drowning coastal plain, where a tidal phase lag generates offshore migration, balancing the wave-driven onshore migration, resulting in a dynamically stable chenier.

offshore. Without a phase lag, only 4% of the model realisations lead to chenier dissolution, and with a phase lag of $\theta = 5$ min, this is the case for less than 1%.

In summary, the storm reset's main effect is a seaward displacement. Due to this yearly seaward displacement (and consequent lowering), the chenier remains more dynamic, even if the crest reached a high enough elevation to prevent submergence by regular tides during the SE monsoon season. Throughout the year, the chenier's behaviour is still dominated by the interaction between the waves, tide and a possible phase lag.

As a final step, all the processes and short-term dynamics described above are combined to investigate the long-term dynamics (10 years), and possible stable chenier states. First, a 'classic' chenier is modelled, without phase lag or storm reset (see Fig. 10a). The chenier migrates

onshore, and the crest level increases until it is close to the highest tidal levels. Once it reaches this high elevation, the onshore migration becomes more episodic, requiring very high tides to submerge the chenier before it can become mobile again. When the chenier is mobile, it follows the pattern of alternating strong onshore migration and local heightening. The chenier does not become as high as classically observed on coastal plains (Augustinus, 1989; Otvos, 2019; Quaresma et al., 2007; Morales et al., 2014; Woodroffe et al., 1983) because we do not account for storm surges in the boundary conditions.

When including a phase lag ($\theta = 5$ min) and yearly storm reset ($\Delta x_{st} = 100$ m), the net horizontal displacement of the chenier is much smaller (see Fig. 10b). The onshore migration is counterbalanced by the gradual effect of the phase lag, and the yearly setback of the storm reset. Both also lower the chenier crest, and therefore increase the submergence time of the chenier, further increasing its dynamics. While initially the chenier migrates onshore, eventually a stable position is found, with the crest around MSL. At intra-annual scales (see dots for chenier location per month) the chenier is still very dynamic, both horizontally and vertically (in agreement with field observations of the chenier, see Fig. 2e), but over annual to decadal scales its average position remains stable (consistent with satellite images, see Fig. 2a-d). This dynamic behaviour is visualised in Fig. 11, where Fig. 11a shows a situation without subsidence (no tidal phase lag), and Fig. 11b shows the behaviour on a drowning coastal plain (with a tidal phase lag).

4. Discussion

As shown in Fig. 10, the idealised chenier model is able to capture trends in chenier geometry under both onshore and offshore migration, mimicking trends we have observed in Demak and have been described in literature for cheniers at other locations around the world. Besides the trend, it is also interesting to compare the magnitude of the migration speeds. For the scenario without phase lag or storm reset the chenier moves on average 500 m landward over 10 years, or 50 m/y (see Fig. 9a). This is the same order of magnitude as migration speeds observed in Korea (Kim et al., 2020) and France (Weill et al., 2012). Fig. 10a shows that the migration speed varies over time, with monthly migration speeds varying strongly over the year. The largest onshore migration computed is around 40 m in one month. It is difficult to compare this value to values in literature, since most recordings cover much longer periods (over a year); the highest monthly migration speeds in literature (when averaging the recorded migration per month) are 17.5 m/month (351 m over 20 months in Saltés Island chenier plain, Spain, Morales et al. (2014)) and 13.6 m/month (95 m over 7 months in Firth of Thames, New Zealand, Woodroffe et al. (1983)). In Demak, the chenier moved 17 m in 10 days during a period of strong onshore migration (see Fig. 2e), which would equal 51 m/month.

In this model set-up, two processes are capable of transporting the chenier offshore: the phase lag and the storm reset. While the phase lag has only a small effect over one tidal cycle, it takes place continuously, resulting in a large effect over longer time; the storm reset only occurs once a year, applying a large offshore displacement at once. We argue that both processes together are responsible for counterbalancing the onshore chenier migration in Demak. Scenarios with a storm reset ($\Delta x_{st} > 0$ m) but without phase lag ($\theta = 0$ min), see Fig. 9c-d, show that, while it is possible to have a stable position over a long term for a large enough storm reset, the horizontal distribution is very broad. This means that such scenarios are relatively easily disturbed, and may not return to previous (equilibrium) positions. Scenarios with a phase lag ($\theta > 0$ min) but without storm reset ($\Delta x_{st} = 0$ m), see Fig. 9a-b, reveal that only for a narrow range of θ an equilibrium is reached; while smaller values of θ invariably lead to onshore migration and lowering (until the chenier becomes a very wide, thin layer of sand on top of the muddy subsurface and dissolves), larger values result in transport of the chenier offshore. However, combining both a non-zero phase lag ($\theta > 0$ min) and a non-zero storm-reset ($\Delta x_{st} > 0$ m), yields a chenier which is very dynamic on the short term, but stable on the long term, and is able to recover from disturbances. Such a dynamic equilibrium can be obtained for different combinations of θ and Δx_{st}. We do not know the exact value of θ and Δx_{st}, and it is also highly probably that these vary over time (for example in response to the monsoon seasons, or due to continuing subsidence). However, on longer time scales the cheniers in Demak are stable, from which it may be concluded that both $\theta > 0$ min and $\Delta x_{st} > 0$ m. If not, only very specific combinations of boundary conditions would yield long-term stability, and this would require the absence of any form of disturbance.

It is interesting to note the similarities and differences between cheniers and breaker bars. While they occur in different environments (cheniers occur on muddy coastlines, breaker bars are a feature of sandy coasts), they are both shore-parallel bodies of sand, reducing wave impact on the coastline. Classic cheniers are known to migrate onshore only, while breaker bars move slowly onshore under mild wave conditions and rapidly offshore under higher wave conditions (Wright and Short, 1984). Eventually, cheniers will become part of the coastline, as they migrate higher up the beachface until they reach above the highest water levels. Breaker bars, on the other hand, will migrate offshore until they reach the limit of the surf zone where they dissolve. Interestingly, the cheniers in Demak seem to posses properties of both 'classic' cheniers and breaker bars, showing both onshore and offshore migration. The model is able to capture all these dynamics, providing an explanation for the driving processes behind them.

A recommendation for future research would be to measure the chenier dynamics in Demak for a wider range of conditions (so also during the NW monsoon season), with special attention to the tidal phase lag, such that the values of θ and Δx_{st} are known for more situations. It may also be useful to repeat similar field observations at different locations around the world, since there is a lack of short-term, detailed observations of chenier dynamics during their 'active phase'. Note that this model is developed for existing cheniers; their formation (and occasional dissolution) is not accounted for. For certain scenarios, many model realisations end early, when the chenier migrates onshore and the crest lowers, until it becomes a thin layer of sand on top of the muddy subsurface and the chenier dissolves. Therefore, another recommendation for future research is to investigate the development of cheniers; not only their initial formation, but also what would happen to such flattened cheniers, such that this behaviour can then also be integrated into the idealised chenier model.

The observed chenier in Demak, while very dynamic, maintains a relatively constant geometry, which allows our approach of using a look-up table based on a single, generic profile (see Fig. 5a). However, if the chenier geometry varies strongly, feedback between the geometry and the displacements could be introduced by modelling different chenier geometries in Delft3D, creating multiple look-up tables. Furthermore, these extra model runs, as well as any additional field observations, could eventually be used to go from look-up tables to deterministic algorithms, which could be used to calculate the fluxes between the different chenier components (similar to the barrier island model of Lorenzo-Trueba and Ashton (2014), or the beach-dune model of Hallin et al. (2019)).

The tidal phase lag is found to be one of the important processes in stabilizing the chenier in the nearshore zone. This phase lag is the result of strong coastal erosion and subsidence, which have caused breaches in

the coastline and turned the coastal plain into a large tidal basin. The presence of a chenier in the nearshore creates a buffer against strong wave action, while still letting water and sediment pass. By damping waves, the chenier protects the coastline against further erosion, and as such, the chenier actually generates a negative feedback on the erosion cycle. Moreover, the presence of a chenier could create a window of opportunity for the mangrove coast to restore and expand again, eventually naturally closing the breaches in the coastline. This would cancel the tidal phase lag, which may tip the chenier dynamics to a different stable state, where the chenier migrates onshore until it ends up in the shoreline. However, a small change to the phase lag, for example by closing off (part of) the hinterland by a dike, could disturb this chenier equilibrium. The dike would strongly reduce the tidal phase lag, which in turn reduces the seaward sediment transport, and the chenier would start migrating onshore. Attached to the shoreline, the chenier no longer creates a sheltered area for mangrove restoration, and there may be local deepening seaward of the chenier, which could eventually lead to aggravated coastal erosion. And finally, if the subsidence continues, the phase lag could even increase, until the seaward transport becomes dominant and the chenier migrates further offshore, leaving the shoreline unprotected.

5. Conclusions

Chenier dynamics on a day-to-day basis are driven by waves and tides. Most cheniers described in literature are known to migrate onshore only, until they stabilise high on the beachface, where they are no longer reached by even the highest tides. Observations in Demak suggest that there may also be an alternative stable state for cheniers, where they remain dynamic on the short-term, but hold a stable position at a certain distance from the shoreline on the longer term.

We have developed an idealised chenier model using output from a complex physics-based model to investigate the drivers of cross-shore chenier dynamics under daily wave and tidal influences. The model is able to capture trends in chenier geometry under both onshore and offshore migration. Onshore migration is mainly driven by wave action. Offshore migration occurs when a phase lag generated on the drowned coastal plain causes a water level gradient over the chenier.

Both the tide and waves may vary over the year; waves due to seasonal effects, tide due to the interaction between the various tidal components. During the SE monsoon season in Demak, the wave climate is driven by a very regular sea breeze. Due to the mixed, mainly diurnal character of the tide, the timing of high water levels shifts over the day throughout the year. This leads to a yearly pattern in chenier dynamics, where based on the timing of the sea breeze vs. the high tide, a period of strong onshore migration is followed by a period of local vertical growth.

Without a tidal phase lag or storm reset, the model reproduces the typical chenier dynamics of strong onshore migration, until the chenier reaches a height that can no longer be reached by daily tidal influences: the ‘classic’ stable state. Introducing a phase lag (caused by subsidence of the coastal plain) and storm reset (representing the net seaward displacement during the storm season) to the boundary conditions strongly impacts these chenier dynamics. Both introduce an offshore transport component, counterbalancing the onshore migration. While either process alone can produce a dynamically stable chenier, this stable position only occurs for a very narrow range of boundary conditions, and the equilibrium is easily disturbed. Both processes together, however, create a more robust equilibrium: very dynamic on the short term, due to the natural variation in boundary conditions, but stable on the long term: an alternative, dynamically stable state.

List of symbols

α	beachface slope [−]
β	muddy substrate slope [−]
Δx	horizontal hourly displacement of the chenier center [m/h]
Δx_{st}	horizontal offshore migration as result of NW monsoon (storm) season [m]
Δz	vertical hourly displacement of the chenier center (including vertical correction) [m/h]
Δz_{D3D}	vertical hourly displacement of the chenier center derived from Delft3D [m/h]
η	water level [m above MSL]
θ	tidal phase lag between seaward and landward model boundary [min]
$_B$	subscript indicating the toe of the back-barrier face
$_C$	subscript indicating the center of the chenier
d_{top}	water depth on top of the chenier crest [m]
H	height of the chenier crest [m]
$H_{s,\infty}$	deep water significant wave height [m]
MSL	Mean Sea Level
$_S$	subscript indicating the beachface toe
$_T$	subscript indicating the chenier toe
x	horizontal coordinate [m]
x'	horizontal correction during chenier evolution in order to guarantee conservation of volume [m]
z	vertical coordinate [m above MSL]
z'	vertical correction during chenier evolution in order to guarantee conservation of volume [m]
z_{corr}	vertical correction to vertical hourly displacement derived from D3D [m/h]

Data availability

The measurement data is available in the repository of 4TU. ResearchData, with the doi: https://doi.org/10.4121/13177388.v1.

Funding

This work is part of the BioManCO project with project number 14753, which is (partly) financed by NWO Domain Applied and Engineering Sciences, and co-financed by Boskalis Dredging and Marine Experts, Van Oord Dredging and Marine Contractors bv, Deltares, Witteveen+Bos and Wetlands International.

Declaration of Competing Interest

The authors declare that they have no known competing financial interests or personal relationships that could have appeared to influence the work reported in this paper.

Acknowledgements

The BioManCO project, initiated and coordinated by Han Winterwerp, is a collaboration between Delft University of Technology, Royal Netherlands Institute for Sea Research (NIOZ) and Center for Coastal Rehabilitation and Disaster Mitigation Studies (CoREM) at Universitas Diponegoro (UNDIP), and makes use of the framework set up by Building with Nature Indonesia, a programme by Ecoshape, Wetlands International, the Indonesian Ministry of Marine Affairs and Fisheries (MMAF), the Indonesian Ministry of Public Works and Housing (PUPR) and other partners. We would also like to thank three anonymous reviewers and the editor for their constructive feedback resulting in an improved paper.

Appendix A. Hourly horizontal and vertical displacements for all scenarios

The idealised chenier model is valid for calm to moderate conditions, representative for the SE monsoon season in Demak. Therefore, the hourly horizontal and vertical hourly displacements for a representative range of conditions have been determined with the Delft3D model: (1) $H_{s,\infty} = 0 - 2$ m; (2) $d_{top} = 0 - 2$ m; (3) ebb or flood; and (4) $\theta = 0 - 20$ min. In the main text, Fig. 6, the hourly displacements for all wave heights and water depths of two sets of scenarios have been shown: ebb without a phase lag (Fig. 6a-b); and ebb with a phase lag of $\theta = 10$ min (Fig. 6c-d). Here, we include the remaining scenarios: flood (Fig. A.12a-b); ebb with a phase lag of $\theta = 5$ min (Fig. A.12c-d); and ebb with a phase lag of $\theta = 20$ min (Fig. A.12e-f).

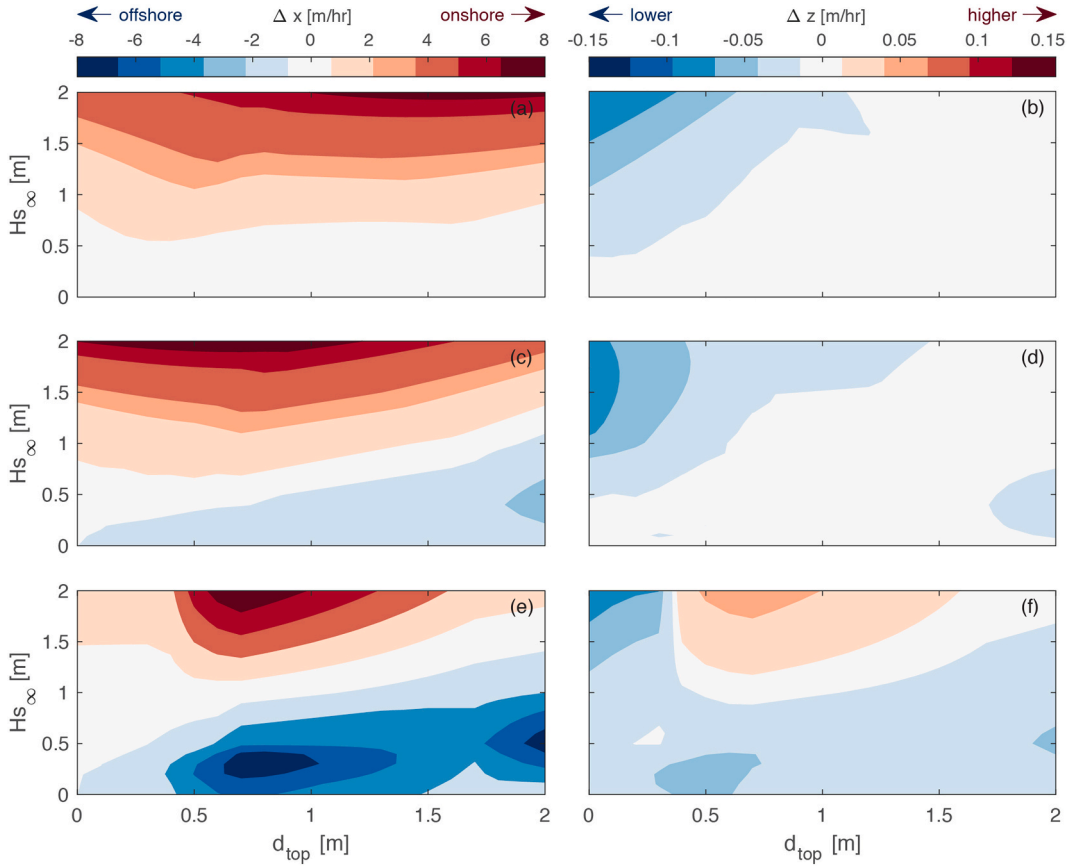

Fig. A.12. Visualisation of the hourly displacement matrix for the scenarios not covered in the main article (see Fig. 6). The first row (**(a)** and **(b)**) shows the displacements during flood; the second row (**(c)** and **(d)**) during ebb with a phase lag of $\theta = 5$ min; and the third row (**(e)** and **(f)**) during ebb with a phase lag of $\theta = 20$ min. The left column (**(a)**, **(c)** and **(e)**) gives the horizontal hourly displacement Δx in m/h, where onshore migration is coloured red and offshore blue; the right column (**(b)**, **(d)** and **(f)**) gives the vertical hourly displacement Δz in m/h, where red colours indicate that the chenier crest becomes higher, while for blue colours the crest lowers. (For interpretation of the references to colour in this figure legend, the reader is referred to the web version of this article.)

References

Abidin, H.Z., Andreas, H., Gumilar, I., Sidiq, T.P., Fukuda, Y., Andreas, H., Gumilar, I., Sidiq, T.P., Land, Y.F., 2013. Land subsidence in coastal city of Semarang (Indonesia): characteristics, impacts and causes. Geomat. Nat. Hazards Risk 4, 226–240. https://doi.org/10.1080/19475705.2012.692336.

Anthony, E.J., Gardel, A., Gratiot, N., Proisy, C., Allison, M.A., Dolique, F., Fromard, F., 2010. The Amazon-influenced muddy coast of South America: a review of mud-bank-shoreline interactions. Earth Sci. Rev. 103, 99–121. https://doi.org/10.1016/j.earscirev.2010.09.008.

Anthony, E.J., Gardel, A., Dolique, F., Marin, D., 2011. The Amazon-influenced mud-bank coast of South America: an overview of short- to long-term morphodynamics of 'inter-bank' areas and chenier development. J. Coast. Res. ICS 2011, 25–29. URL: https://www.jstor.org/stable/26482126.

Anthony, E.J., Gardel, A., Gratiot, N., Guiana, F., 2013. Fluvial sediment supply, mud banks, cheniers and the morphodynamics of the coast of South America between the Amazon and Orinoco river mouths. In: Martini, I.P., Wanless, H.R. (Eds.), Geological Society, London, vol. 388. The Geological Society of London, pp. 533–560. Special Publications.

Anthony, E.J., Brunier, G., Gardel, A., Hiwat, M., 2019. Chenier morphodynamics on the Amazon-influenced coast of Suriname, South America: implications for beach ecosystem services. Front. Earth Sci. 7, 1–20. https://doi.org/10.3389/feart.2019.00035.

Augustinus, P.G.E.F., 1980. Actual development of the chenier coast of Suriname (South America). Sediment. Geol. 26, 91–113. https://doi.org/10.1016/0037-0738(80)90007-X.

Augustinus, P.G.E.F., 1989. Cheniers and chenier plains: a general introduction. Mar. Geol. 90, 219–229. https://doi.org/10.1016/0025-3227(89)90126-6.

Bayliss-Smith, T.P., Healey, R., Lailey, R., Spencer, T., Stoddart, D.R., 1979. Tidal flows in salt marsh creeks. Estuar. Coast. Mar. Sci. 9, 235–255.

Brunier, G., Anthony, E.J., Gratiot, N., Gardel, A., 2019. Exceptional rates and mechanisms of muddy shoreline retreat following mangrove removal. Earth Surf. Process. Landf. 44, 1559–1571. https://doi.org/10.1002/esp.4593.

Cohn, N., Hoonhout, B.M., Goldstein, E.B., de Vries, S., Moore, L.J., Durán Vinent, O., Ruggiero, P., 2019. Exploring marine and aeolian controls on coastal foredune growth using a coupled numerical model. J. Mar. Sci. Eng. 7 https://doi.org/10.3390/jmse7010013.

Dubarbier, B., Castelle, B., Marieu, V., Ruessink, G., 2015. Process-based modeling of cross-shore sandbar behavior. Coast. Eng. 95, 35–50. https://doi.org/10.1016/j.coastaleng.2014.09.004.

Ervita, K., Marfai, M.A., 2017. Shoreline change analysis in Demak, Indonesia. J. Environ. Prot. 08, 940–955. https://doi.org/10.4236/jep.2017.88059.

Fitrianti, N., Harryanto, Y.D., Simamora, E.V.S., Bintari, H.F.A., Hartoko, A., Anggoro, S., Zainuri, M., 2018. Analysis of daily wind circulation toward sea level rise in Semarang. In: IOP Conference Series: 1st International Conference on Maritime Sciences and Advanced Technology "Ocean Science and Technology Toward a Global Maritime Axis". IOP, pp. 1–11.

Flanders Marine Institute (VLIZ), Intergovernmental Oceanographic Commission (IOC), 2021. Sea Level Monitoring Facility. https://doi.org/10.14284/482. http://www.ioc-sealevelmonitoring.org (Accessed on 2021-07-20).

French, J., Payo, A., Murray, B., Orford, J., Eliot, M., Cowell, P., 2016. Appropriate complexity for the prediction of coastal and estuarine geomorphic behaviour at

decadal to centennial scales. Geomorphology 256, 3–16. https://doi.org/10.1016/j.geomorph.2015.10.005.
Friedrichs, C.T., 2010. Barotropic tides in channelized estuaries. In: Valle-Levinson, A. (Ed.), Contemporary Issues in Estuarine Physics. Cambridge University Press, Cambridge, UK, pp. 27–61.
Friedrichs, C.T., Madsen, O.S., 1992. Nonlinear diffusion of the tidal signal in frictionally dominated embayments. J. Geophys. Res. 97, 5637–5650.
Google Earth, 2021. Satellite Images of Demak, Indonesia Between 1994 and 2020. https://earth.google.com/web/ (Accessed 2021-06-05).
Hallin, C., Larson, M., Hanson, H., 2019. Simulating beach and dune evolution at decadal to centennial scale under rising sea levels. PLoS One 14. https://doi.org/10.1371/journal. pone.0215651.
Heward, A.P., 1981. A review of wave-dominated clastic shoreline deposits. Earth Sci. Rev. 17, 223–276.
Horstman, E.M., Dohmen-Janssen, C.M., Hulscher, S.J.M.H., 2013. Flow routing in mangrove forests: a field study in Trang province, Thailand. Cont. Shelf Res. 71, 52–67. https://doi.org/10.1016/j.csr.2013.10.002.
Horstman, E.M., Bryan, K.R., Mullarney, J.C., 2021. Drag variations, tidal asymmetry and tidal range changes in a mangrove creek system. Earth Surf. Process. Landf. 1–19. https://doi.org/10.1002/esp.5124.
Kim, D., Jo, J., Kim, B., Ryu, J., Choi, K., 2020. Influence of dike-induced morphologic and sedimentologic changes on the benthic ecosystem in the sheltered tidal flats, Saemangeum area, west coast of Korea. Environ. Pollut. 257, 113507 https://doi.org/10.1016/j.envpol.2019.113507.
Kuehn, F., Albiol, D., Cooksley, G., Duro, J., Granda, J., Haas, S., Hoffmann-Rothe, A., Murdohardono, D., 2010. Detection of land subsidence in Semarang, Indonesia, using stable points network (SPN) technique. Environ. Earth Sci. 60, 909–921. https://doi.org/10.1007/s12665-009-0227-x.
Lang, C., 1869. Kaart van den spoorweg van Samarang naar de Vorstenlanden. http://hdl.handle.net/1887.1/item:811882.
Lee, H.J., Chun, S.S., Chang, J.H., Han, S.J., 1994. Landward migration of isolated Shelly Sand Ridge (Chenier) on the macrotidal flat of Gomso Bay, West Coast of Korea: controls of storms and typhoon. J. Sediment. Res. A64, 886–893.
Lesser, G.R., Roelvink, J.A., van Kester, J.A.T.M., Stelling, G.S., 2004. Development and validation of a three-dimensional morphological model. Coast. Eng. 51, 883–915. https://doi.org/10.1016/j.coastaleng.2004.07.014.
Lorenzo-Trueba, J., Ashton, A.D., 2014. Rollover, drowning, and discontinuous retreat: Distinct modes of barrier response to sea-level rise arising from a simple morphodynamic model. J. Geophys. Res. 119, 779–801. https://doi.org/10.1002/2013JF002871.Received.
Marfai, M.A., Tyas, D.W., Nugraha, I., 2016. The morphodynamics of Wulan Delta and its impacts on the coastal community in Wedung subdistrict, Demak regency, Indonesia. J. Environ. Prot. 7, 60–71.
Mazda, Y., Kanazawa, N., Wolanski, E., 1995. Tidal asymmetry in mangrove creeks. Hydrobiologia 295, 51–58. https://doi.org/10.1007/BF00029110.
Morales, J.A., Borrego, J., Davis, R.A., 2014. A new mechanism for chenier development and a facies model of the Saltés Island chenier plain (SW Spain). Geomorphology 204, 265–276. https://doi.org/10.1016/j.geomorph.2013.08.011.
Murray, A.B., 2003. Contrasting the Goals, strategies, and predictions associated with simplified numerical models and detailed simulations. In: Wilcock, P.R., Iverson, R. M. (Eds.), Prediction in Geomorphology. American Geophysical Union (AGU), pp. 151–165. https://doi.org/10.1029/135GM11.
Nardin, W., Fagherazzi, S., 2018. The role of waves, shelf slope, and sediment characteristics on the development of Erosional Chenier Plains. Geophys. Res. Lett. 45, 8435–8444. https://doi.org/10.1029/2018GL078694.
Neal, A., Richards, J., Pye, K., 2002. Structure and development of shell cheniers in Essex, southeast England, investigated using high-frequency ground-penetrating radar. Mar. Geol. 185, 435–469. https://doi.org/10.1016/S0025-3227(01)00239-0.
Otvos, E.G., 2019. Cheniers. In: Finkl, C.W., Makowski, C. (Eds.), Encyclopedia of Coastal Science. Springer Nature, Switzerland, pp. 1–5. https://doi.org/10.1007/978-3-319-48657-4_67–5.
Otvos, E.G., Price, W.A., 1979. Problems of chenier genesis and terminology - an overview. Mar. Geol. 31, 251–263.
Parker, G., Muto, T., 2003. 1D numerical model of delta reponse to rising sea level. In: Sánchez-Arcilla, A., Bateman, A. (Eds.), 3rd IAHR Symposium on River, Coastal and Estuarine Morphodynamics (RCEM). International Association of Hydraulic Engineering and Research, Barcelona, Spain, pp. 1–10.
Quaresma, V.D.S., Bastos, A.C., Amos, C.L., 2007. Sedimentary processes over an intertidal flat: a field investigation at Hythe flats, Southampton Water (UK). Mar. Geol. 241, 117–136. https://doi.org/10.1016/j.margeo.2007.03.009.
Rhodes, E.G., 1982. Depositional model for a chenier plain, Gulf of Carpentaria, Australia. Sedimentology 29, 201–221.
Russell, R.J., Howe, H.V., 1935. Cheniers of Southwestern Louisiana. Geogr. Rev. 25, 449–461. https://doi.org/10.1016/S0167-8116(15)00050-6.
Ryu, J.H., Kim, C.H., Lee, Y.K., Won, J.S., Chun, S.S., Lee, S., 2008. Detecting the intertidal morphologic change using satellite data. Estuar. Coast. Shelf Sci. 78, 623–632. https://doi.org/10.1016/j.ecss.2008.01.020.
Spaans, L., 2019. Cross-shore Morphodynamics of Intertidal Sandbars. Msc thesis. Delft University of Technology. http://resolver.tudelft.nl/uuid:7f0fe44f-4f8a-44b7-9bbd-23043e1a8e68.
Tas, S.A.J., van Maren, D.S., Reniers, A.J.H.M., 2020. Observations of cross-shore chenier dynamics in Demak, Indonesia. J. Mar. Sci. Eng. 8 https://doi.org/10.3390/jmse8120972.
Taylor, M., Stone, G.W., 1996. Beach-ridges: a review. J. Coast. Res. 12, 612–621.
Temmerman, S., Bouma, T.J., Govers, G., Wang, Z.B., de Vries, M.B., Herman, P.M.J., 2005. Impact of vegetation on flow routing and sedimentation patterns: Three-dimensional modeling for a tidal marsh. J. Geophys. Res. 110 https://doi.org/10.1029/2005JF000301.
Toorman, E.A., Anthony, E.J., Augustinus, P.G.E.F., Gardel, A., Gratiot, N., Homenauth, O., Huybrechts, N., Monbaliu, J., Moseley, K., Naipal, S., 2018. Interaction of mangroves, coastal hydrodynamics, and morphodynamics along the coastal fringes of the Guianas. In: Makowski, C., Finkl, C.W. (Eds.), Threats to Mangrove Forests, vol. 20. Springer, pp. 429–473. https://doi.org/10.1007/978-3-319-73016-5_20.
van Bijsterveldt, C.E.J., 2021. A Peak Into the Future of Densely Inhabited Low-lying Coastal Areas: The Impact of Land-subsidence (Working Title) (Manuscript in preparation).
van Bijsterveldt, C.E.J., van der Wal, D., Gijón Mancheño, A., Fivash, G., Helmi, M., Bouma, T.J., 2021. Can Cheniers Protect Mangroves along Eroding Coastlines? The Effect of Contrasting Foreshore-types on Mangrove Stability (Manuscript submitted for publication).
van Duin, M.J.P., Wiersma, N.R., Walstra, D.J.R., van Rijn, L.C., Stive, M.J.F., 2004. Nourishing the shoreface: observations and hindcasting of the Egmond case, the Netherlands. Coast. Eng. 51, 813–837. https://doi.org/10.1016/j.coastaleng.2004.07.011.
Weill, P., Tessier, B., Mouazé, D., Bonnot-Courtois, C., Norgeot, C., 2012. Shelly cheniers on a modern macrotidal flat (Mont-Saint-Michel bay, France) - internal architecture revealed by ground-penetrating radar. Sediment. Geol. 279, 173–186. https://doi.org/10.1016/j.sedgeo.2010.12.002.
Winterwerp, J.C., Albers, T., Anthony, E.J., Friess, D.A., Gijón, A., Moseley, K., Muhari, A., Naipal, S., Noordermeer, J., Oost, A., Saengsupavanich, C., Tas, S.A.J., Tonneijck, F.H., Wilms, T., Bijsterveldt, C.V., Eijk, P.V., Lavieren, E.V., Wesenbeeck, B.K.V., 2020. Managing erosion of mangrove-mud coasts with permeable dams – lessons learned. Ecol. Eng. 158, 106078 https://doi.org/10.1016/j.ecoleng.2020.106078.
Woodroffe, C.D., Grime, D., 1999. Storm impact and evolution of a mangrove-fringed chenier plain, Shoal Bay, Darwin, Australia. Mar. Geol. 159, 303–321. https://doi.org/10.1016/S0025-3227(99)00006-7.
Woodroffe, C.D., Curtis, R.J., Mclean, R.F., 1983. Development of a chenier plain, Firth of Thames, New Zealand. Mar. Geol. 53, 1–22. https://doi.org/10.1016/0025-3227(83)90031-2.
Wright, L.D., Short, A.D., 1984. Morphodynamic variability of surf zones and beaches: a synthesis. Mar. Geol. 56, 93–118. https://doi.org/10.1016/0025-3227(84)90008-2.